Coordinated Control of a Hybrid-Electric-Ferry Shipboard Microgrid

Zhao-xia, Xia; Tianli, Zhu; Huaimin, Li; Guerrero, Josep M.; Su, Chun-Lien; Vasquez, Juan C.

Published in:
IEEE Transactions on Transportation Electrification

DOI (link to publication from Publisher):
10.1109/TTE.2019.2928247

Publication date:
2019

Document Version
Accepted author manuscript, peer reviewed version

This article has been accepted for publication in a future issue of this journal, but has not been fully edited. Content may change prior to final publication. Citation information: DOI 10.1109/TTE.2019.2928247, IEEE Transactions on Transportation Electrification

Coordinated Control of a Hybrid-Electric-Ferry Shipboard Microgrid

Xiao Zhao-xia, Zhu Tianli, Li Huaimin, Josep M. Guerrero, *Fellow, IEEE*, Chun-Lien Su, *Member, IEEE*, Juan C. Vásquez, Senior *Member,IEEE*

***Abstract*—DC and DC/AC hybrid distribution and energy storage for shipboard power systems (SPS) are becoming a major trend due to efficiency improvement, space saving, and maneuverability enhancement. This paper has taken a real hybrid-electric-ferry as a case-study to integrate battery units (BUs) to a DC bus for supplying the propulsion motors. Further, two diesel generators (DGs) are connected to the AC bus to supply the hotel loads and a bidirectional DC/AC converter with an *LCL* filter is responsible for the power flow between AC and DC buses. This power topology is flexible for this ferry operation in pure electric, range extended and shore power modes. DC bus voltage is stabilized and its voltage ripple is limited by BUs' interleaved three-phase bidirectional DC/DC converter with its controller considering the operation states of propulsion motors. A coordinated power flow control between DGs and BUs is presented that the system frequency is fixed for the optimal operational efficiency of the diesel engines and a *Q-V* droop control plus a virtual impedance loop is used to make different AC bus voltage. Synchronization with shore power and DC/AC converter is facilitated by *P-f* droop control. Simulation results are presented to validate the proposed control approach in different missions.**

***Index Terms*—Shipboard Microgrid, Hybrid electric ferry, Coordinated control, Propulsion load, Impedance-based stability**

I. INTRODUCTION

Driven by the increased onboard electrical power demand and the progressively stricter environmental requirements, the maritime industry is developing new solutions for the future vessels [1]-[2]. In the 1980s, power electronic converters (PECs) have made a breakthrough in the field of marine vessels by enabling electrification of the propulsion systems due to the introduction of variable-voltage variable-frequency drive technologies [3], [5]. The first change occurred with the introduction of electrical propulsion system aboard in Queen Elizabeth II in the late 1980s, in which 35% of fuel saving was recorded [4]. The advantages obtained from PECs, including maneuverability improvement and space saving, have resulted in the current tendency to further electrify the vessel, namely more-electric ship (MES) or all-electric ship (AES) [6]. Inspired by the success obtained, the concept of all-electric ships was firstly proposed by the U.S. Navy to meet the unprecedented increasing electrical power demand of modern naval vessels [7]-[9] and then adopted in other kinds of civilian vessels [10]-[11]. In addition to the use of electric propulsion, the most important change is the integrated power system (IPS) design [12], in which the power generated aboard a vessel is now available for all the onboard systems instead of being exclusive for either propulsion or ship services loads.

An overwhelming majority of existing vessels are based on AC distribution, while the recent progress of power electronics and energy storage devices specifically drives the development of DC distribution and DC/AC hybrid distribution vessels [13]-[15]. It can further improve fuel consumption efficiency and facilitate access to energy storage compared to AC shipboard power system. In 2011, ABB launched globally the DC onboard grid technology [16]. In 2013, it was successfully applied the technology to the "Dina Star" that variable-speed diesel synchronous generator sets are used and diesel engines can operate at high-efficiency points in the 35%-85% load range[17]-[18]. This fact showed that the use of DC distribution technology can save up to 27% of fuel, and 14% more of fuel can be saved in Dynamic Position (DP) mode, while the engine room noise can be reduced by 30%. Afterward, Siemens launched its new-generation DC ship "BlueDrive PlusC" that the DC electric propulsion system uses a specially designed brushless synchronous generator and the engines can set its speed at each moment according to the required torque and the optimal fuel consumption curve so that it can run at the optimal energy efficiency. Its latest "Odin's Eye" DC uses the existing four-quadrant power converter to form a DC ring network, and each DC power supply area is connected to the ring network, which can achieve high redundancy and fast short circuit protection[19]. Furthermore, Siemens used diesel generator (DG) sets and batteries mixed in DC shipboard power system (SPS) for an offshore support vessel named "Edda Ferd". In that one, it was claimed that the use of batteries can further reduce fuel consumption of SPS, especially in DP modes [20]. Both ABB and Siemens use synchronous generator sets and diode rectifier to the DC bus. In 2009, German E-MS Company used variable-speed diesel asynchronous generator sets and a full-controlled rectifier connected to the DC bus, claiming that

This work was supported by the Tianjin Science and Technology Support Program Key Project (17JCZDJC31300).

Xiao Zhao-xia, Zhu Tianli and Li Huaimin are with Tianjin Key Laboratory of Advanced Electrical Engineering and Energy Technology, Tianjin Polytechnic University, Tianjin, 300387, P. R. China (xiaozhaoxia@tjpu.edu.cn).

Su Chuncheng is in department of Marine Engineering, National Kaohsiung University of Science and Technology, Kaohsiung City, Taiwan, 805 (cls@nkust.edu.tw)

Josep M. Guerrero and Juan C. Vasquez are in Department of Energy Technology, Aalborg University, Denmark, 9220 . Josep M. Guerrero was funded by a Villum Investigator grant (no. 999730) from The Villum Foundation. (joz@et.aau.dk, juq@et.aau.dk) .

This article has been accepted for publication in a future issue of this journal, but has not been fully edited. Content may change prior to final publication. Citation information: DOI 10.1109/TTE.2019.2928247, IEEE Transactions on Transportation Electrification

generators can achieve higher energy efficient operation in an 85% speed range [19] and the first DC distribution ship "Rainbowfish" was commissioned in China last year [21]. DC/AC hybrid distribution is relatively rare and it mainly used in ferries. Kaohsiung Port of Taiwan announced that they will renovate their ferries to DC/AC hybrid distribution and the batteries will serve as the main source of ferries. The typical structures of AC and DC distribution shipboard power system are shown in Fig.1.

The SPS is essentially an independently operated microgrid (MG), called Shipboard Microgrids (SMGs). The SMGs becomes more or less similar to Land-based Microgrids (LMGs). The common characteristics between the SMGs and LMGs include islanded operation, increased use of power electronic converters and network architectures. Therefore, some technologies developed for islanded LMGs can be extended for SMGs as well [21-22]. Nevertheless, there are also many differences: (1) The general SMGs whose power generation system is mainly diesel generator sets, the load is mainly the dynamic propulsion and pump loads account for about 70% of the total load power, and its power variation will influence the power system stability (2) The space on the ship is limited, so the volume and weight of its power equipment are relatively small; (3) wind and ocean current will impact on the stability, reliability, and survivability of the shipboard power system. The similarities and differences between SMGs and LMGs are shown in TABLE I. So SMGs have become more complex in coordinated control, stability analysis and power management [23-25].

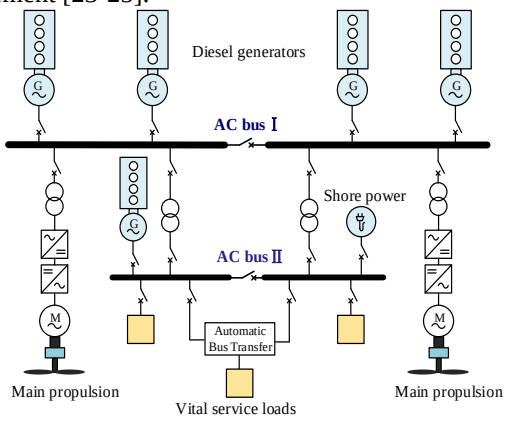

(a) AC distribution

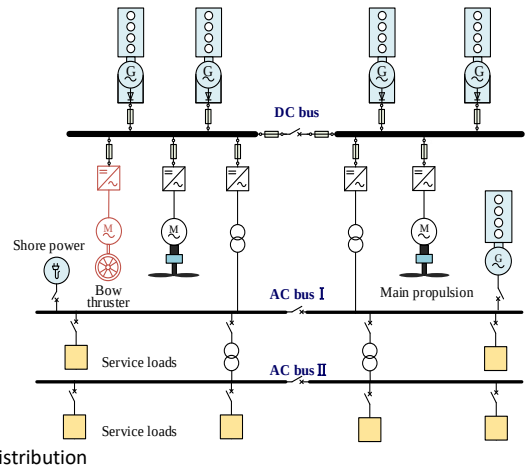

(b) DC distribution

Fig. 1. Typical structures of AC and DC distribution shipboard power system.

TABLE I SIMILARITIES AND DIFFERENCES BETWEEN SMGS AND LMGS.

		LMGs	SMGs
Similarity		• Islanded operation • Increased use of power electronic converters • Network architectures	
Difference	Energy sources	Intermittent renewable energy	Diesel, liquid natural gas
	Loads	Regular loads	Dynamic propulsion and pump loads
	Size and weight	Not critical	Critical
	Stability, reliability and survivability	Not very high	High

A lot of research has been done in islanded MG control, aiming to balance active power (P) and reactive power (Q) between generators and loads, thus making MGs to operate as a relatively large controlled voltage source [21], [26-28]. According to the type of power supply, MGs are divided into AC, DC, and AC/DC hybrid ones. The essence of AC/DC hybrid MG is an AC system, and maintaining voltage and frequency stability is the main control issue. In the case of DC MGs, voltage control is the key issue [29]-[30]. In 2011, the hierarchical control of islanded MGs based on droop-controlled voltage sources are proposed, which can be interesting when connecting a number of energy storages into an islanded MG [21]. Until now, hierarchical control has become a standardized control method in MGs. It can control and optimize the dynamic and stable process of the MG in multiple time scales and multiple target dimensions, ensuring system stability and economy. However, due to the electric propulsion load accounts for about 70% of the total, the coordinated control of the shipboard microgrid must balance stability and efficiency. Stability, high energy efficiency, and low pollution emissions are the main task for a shipboard microgrid. In [31], it is the first time that hierarchical control is introduced into the control of the DC SPS. By using improved droop control, the load power sharing between different power sources is achieved, at the same time, the DC bus voltage quality is improved by the second level control. In [32], the propulsion system is regarded as a constant power load, and the influence of the negative incremental impedance characteristics of the constant power load on the stability of the shipboard microgrid is analyzed.

This paper has taken a real hybrid electric ferry as a research case that “hybrid” means the hybrid power sources and DC/AC distribution structure. The power topology is that the battery units (BUs) connect to the DC bus to supply the propulsion motors by a bidirectional DC/DC converter, two diesel generators (DGs) connect to the AC bus to supply the hotel loads and a bidirectional DC/AC converter with an LCL filter is responsible for the power flow between AC and DC bus. That is flexible for the SMGs operating in three modes including pure electric mode, range-extended mode, and shore power mode. If it operates in pure electric mode, the SMGs is a DC distribution system, to control of the battery-side converter to stabilize the DC bus voltage and limit the discharging current of the BUs is the main task. If it operates in range-extended mode, the SMGs is a DC/AC hybrid power system and the main work are to coordinate the DC/AC converter and the diesel

generator sets. And in shore power mode, it is required charging the BUs in a limited current. Hence, the main goals of this paper are proposed as follows:

1) To design a power topology for the hybrid electric ferry in different operation modes.
2) To design topology of bidirectional DC/DC converter and its controller to keep the DC bus stable when the propulsion motor in different missions.
3) To develop a coordinated control method to improve the fuel consumption efficiency and power quality of the shipboard microgrid.
4) To ensure seamless transition considering various operation scenarios and missions.

The paper is organized as follows. Section II presents the power topology of the hybrid electric ferry. Section III describes pure electric mode including the interleaved three-phase bidirectional DC/DC converter, its two-loop anti-windup PI controller, and the choice of the DC bus capacitor and the controller parameters of the DC/DC converter. Section IV presents range-extended mode that a coordinated control between DGs and BUs is introduced. Section V describes the shore power mode. Section VI presents the simulation results of a hybrid electric ferry in different operation scenarios. Finally, Section VII summarizes this paper.

II. System Model of Hybrid Electric Ferry

The designed electrical structure of the hybrid electric ferry is shown in Fig.2. The BUs are connected to the DC bus by the interleaved three-phase bidirectional DC/DC converter. Two DGs are directly connected to the AC bus. The AC bus and DC bus are connected by bidirectional DC/AC converter with an LCL filter. Two propulsion motors using permanent magnet synchronous motor (PMSM) are connected to the DC bus by its electric drivers. A transformer is used to reduce the voltage for the hotel loads. The normal operation modes include pure electric mode (PEM) and range-extended mode (REM). The shore power is used to supply for the hotel load and to charge the BUs, called shore power mode (SPM).

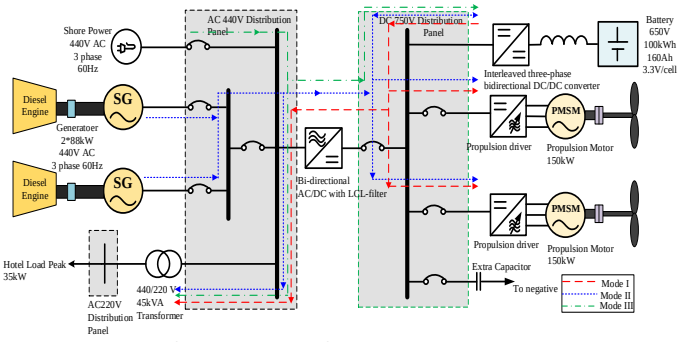

Fig. 2. Structure of hybrid electric ferry.

Mode I (PEM): it refers to a mode of ferry operation that is dependent on energy from the battery units, which the BUs supplies the propulsion motors and the hotel loads, meanwhile, the DGs are disconnected. The shipboard microgrid is a DC distribution power system.

Mode II (REM): the electric ferry switches to range-extended mode after the battery has reached its minimum state of charge (SoC) threshold that exhausts the ferry all-electric range. One advantage of a range-extended mode is that it may afford the ferry designer an opportunity to use a smaller and less costly BUs. The shipboard microgrid is a hybrid DC/AC distribution power system, and DGs supply the propulsion motors and the hotel loads and charge the BUs.

Mode III (SPM): The shore power is to charge the BUs and supply for the hotel load.

III. Pure Electric Mode

A. *Battery DC/DC converter and its controller.*

The interleaved three-phase bidirectional DC/DC converter and its controller is shown in Fig. 3, which is used for the large supply power and small current ripple [32]. A two-loop controller is adapted which the outer loop is the DC bus voltage control to keep the voltage follow the reference, and the inner loop is battery discharging/charging current control, furthermore, the output limit of the outer loop is the maximum allowable discharging/charging current of the battery. An adaptive PI voltage control is employed that different proportional controller parameters for the outer voltage loop in dynamic and steady state. When the voltage error is bigger than 1%, the value of the proportional controller is bigger than that the voltage error is smaller than 1%. And the anti-windup PI controller is for escaping the saturation of the duty cycle when the propulsion motors start and power changes.

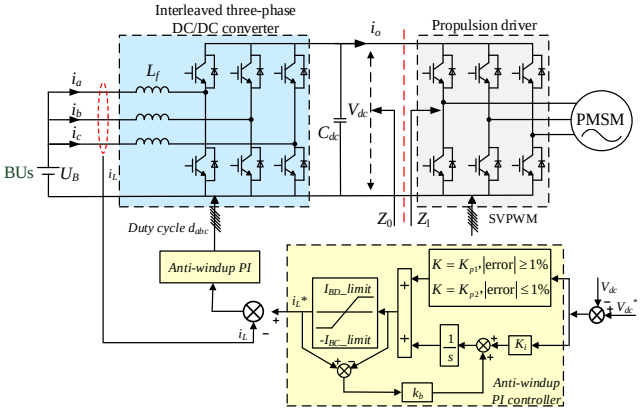

Fig. 3. Battery DC/DC converter and its controller.

B. *PMSM and its DC/AC driver.*

A two-loop controller is used to making the PMSM rotating speed to follow the reference speed that the outer loop is the rotation speed loop and the inner loop is the current control. Due to the propeller characteristics, the mechanical torque of the propulsion motor is $T_m = k\omega^2$, where ω is the rotation speed of the PMSM.

C. *Choice of DC Bus Capacitor and DC/DC Converter Controller Parameters.*

An impedance-based method is used for the choice of the DC bus capacitor and the controller parameters of the DC/DC converter. The parameter choice mainly considers three aspects:

(1) When there is a short-circuit fault between the positive and negative poles of DC bus, the DC bus capacitor will instantaneously provide a large short-circuit current. We hope to choose a smaller DC bus capacitor while maintaining the stability of the DC bus voltage.

(2) The boost DC/DC converter with its controller should keep the system stable and the dynamic response characteristics, and

the ripple of the DC bus voltage should be within the required range when the propulsion load power changes.

(3) The cascade system should be stable and have no resonance due to the propulsion motors with its power electronic driver can be considered as a constant power load from the source terminal. Constant power load has the characteristic of negative increment impedance and may reduce the system damping and cause the system unstable.

The transfer function block of the DC/DC converter with its controller is shown in Fig.4 [33]-[36]. Where, G_{ud} is the open-loop transfer function from the duty cycle d to the DC bus voltage V_{dc}, G_{id} is the open-loop transfer function from the duty cycle d to the inductor current i_l, Z_{op} is the open-loop transfer function from the output current i_o to the DC bus voltage V_{dc}, G_{uu} is the open-loop transfer function from the battery voltage U_b to the DC bus voltage V_{dc}, G_{ii} is the open-loop transfer function from the output current i_o to the inductor current i_l, G_{iu} is the open-loop transfer function from the battery voltage U_b to the inductor current i_l. G_m is the PWM modulation ratio and is usually equal to 1. The outer-loop voltage PI controller of the DC/DC converter can be expressed as G_{PIu} and the inner loop current PI controller can be expressed as G_{PIi}.

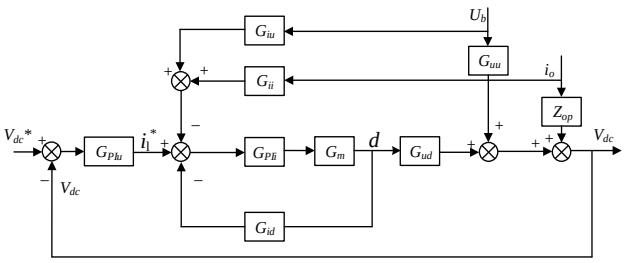

Fig. 4. Transfer function block of the DC/DC converter with its controller.

The closed-loop current transfer function G_{ic} from the inductor reference current i_l^* to the duty cycle d can be expressed as

$$G_{ic} = \frac{G_{PIi}}{1 + G_{id} \cdot G_{PIi}} \tag{1}$$

The open-loop voltage transfer function G_o from the DC bus voltage reference V_{dc}* to the DC bus voltage V_{dc} can be expressed as:

$$G_o = G_{PIu} \cdot G_{ud} \cdot G_{ic} \tag{2}$$

The closed-loop voltage transfer function G_u from the DC bus voltage reference V_{dc}^* to the DC bus voltage V_{dc} can be expressed as:

$$G_u = \frac{V_{dc}}{V_{dc}*} = \frac{G_{ud} \cdot G_{ic} \cdot G_{PIu}}{1 + G_{ud} \cdot G_{ic} \cdot G_{PIu}} \tag{3}$$

The equivalent output impedance Z_o of the DC/DC converter with its controller can be expressed as the following equation:

$$Z_o = \frac{V_{dc}}{-i_o} = \frac{-Z_{op} - G_{ii} \cdot G_{ic} \cdot G_{ud}}{1 + G_{piu} \cdot G_{ic} \cdot G_{ud}} \tag{4}$$

And the transfer function of the constant power load impedance Z_{CPL} can be expressed as:

$$Z_{CPL}(s) = -V_{dc}^2 / P_e \cdot (s + \omega)/\omega \tag{5}$$

The bode plots of the G_o is shown in Fig. 5 when the K_p, and C_{dc} change. From Fig.5 (a), the amplitude and phase stability margin of the G_o will be decreased and the DC bus voltage may be unstable when the K_p increases. And from Fig.5 (b), the amplitude stability margin of the G_o will be increased and the phase stability margin will be decreased and the DC bus voltage ripple will be reduced when the DC bus capacitor C_{dc} increases. However, when the DC bus capacitor changes from 4mF to 14mF, the stability margin has a little change and the DC bus capacitor has little effect on system stability when the propulsion motor uses PMSM. Further, from the step responses of G_u we know the response speed is faster when the voltage PI controller K_p and K_i increases. If the K_p is too big, the system will be unstable.

The equivalent circuit of the cascade system including the DC/DC converter with its controller and the propulsion load is shown in Fig.6. The stability of the cascade system is determined by the equivalent output impedance Z_o and the constant power load impedance Z_{CPL}.

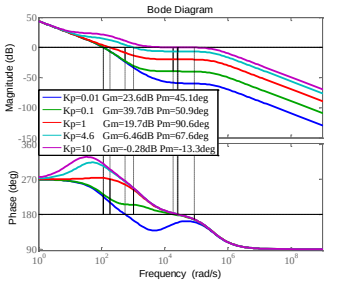

(a) K_p changes and K_i=100, P_e=300kW.

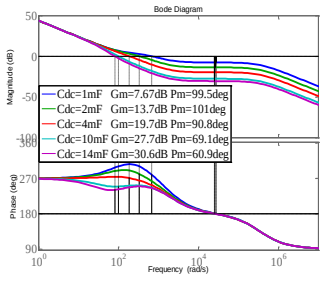

(b) C_{dc} changes and K_p =1, K_i =100, P_e=300kW.

Fig. 5. Bode plots of G_o.

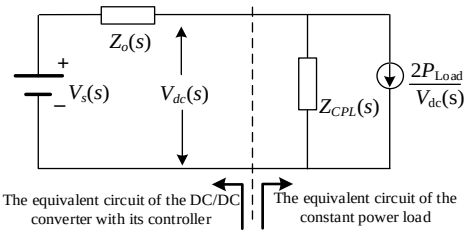

Fig. 6. The equivalent circuit of the cascade system.

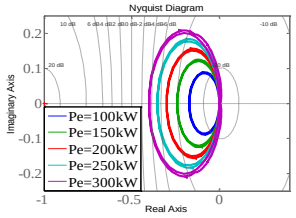

(a) P_e changes and K_p=1 K_i=100, C_{dc}=4mF.

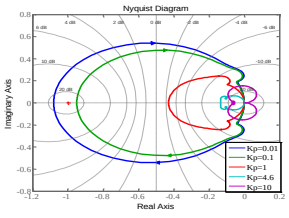

(b) K_p changes and K_i=100, C_{dc}=4mF, P_e=300kW.

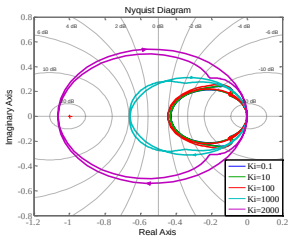

(c) K_i changes and K_p=1, C_{dc}=4mF,P_e =300kW.

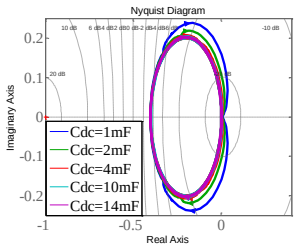

(d) C_{dc} changes and K_p =1, K_i =100, P_e=300kW.

Fig.7. The Nyquist curve of N(s).

The Nyquist curve of transfer function $N(s)=Z_o(s)/Z_{CPL}(s)$ is shown in Fig.7 when the load power and the voltage PI controller K_p, K_i of the DC/DC converter and the DC bus capacitor C_{dc} change. From Fig.7 (a), the constant power load will reduce the damping of the cascade system and the load

capacity will be limited. From Fig.7 (b), the DC part of the hybrid electric ferry will be more stable when the K_p increases. From Fig.7 (c), the system can be stable if the K_i is not too much. From Fig.5 (b) and Fig.7 (d), the extra DC bus capacitor can be zero and only need to keep the fore-stage capacitor of four converters in the hybrid electric ferry.

In summary, considering the stability of the DC/DC converter with its controller and the constant load, the resonance, the response speed, the ripple and harmonics, the fault current of the DC bus, and the limit of the load capacity, the selection of the K_p is in a range, for the case, $0.01 \le K_p \le 5$, and the selection of the K_i should be as large as possible under the premise of the stability of the cascade system. When the voltage error is bigger than 1%, we choose K_p=4.6, K_i=100, and when the proportional controller is bigger than that the voltage error is smaller than 1%, we choose K_p=1, K_i=100. The extra DC bus capacitor can be zero and only need to keep the fore-stage capacitor of four converters. Therefore, we choose C_{dc}=4mF, namely, the extra DC bus capacitor is zero.

In order to limit the ripple of the output voltage, the fore-stage capacitor of each converter is required. According to the formula $C_{dc\_min} = \frac{(1-d)\cdot I_o}{\Delta V_{dc} \cdot f_s}$, when the switching frequency f_s=8 kHz and the ripple factor $\Delta V_{dc}/V_{dc}$ =1%, the minimum capacitor is C_{dc_min} = 0.87 mF. Considering a certain margin of the fore-stage capacitor, we choose each fore-stage capacitor is 1mF.

IV. RANGE EXTENDED MODE

When the hybrid electric ferry operates in Mode II, the SPS is a hybrid AC/DC islanded MG. Maintaining frequency stability and voltage magnitude in the required range is the main issue. At the same time, improving the fuel consumption efficiency of diesel engines and reducing pollution emissions are also important.

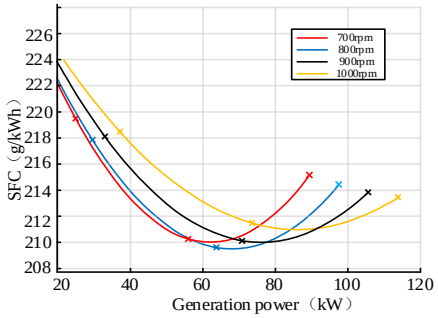

Fig. 8. Relationship between specific fuel consumption, output power and rotation speed of diesel engine.

A. *Principle of coordinated control*

The relationship between specific fuel consumption, generation power, and speed of the diesel engine is shown in Fig.8 [19]. When the output power of diesel engine speed changes, the diesel engine has an optimal operation point for fuel consumption. Generally, the rotation speed of the diesel engine is higher when the output power is bigger at the optimal operation point, namely the mechanical torque is close to the maximum torque.

When the shipboard microgrid operates in Mode II, the controller of DC/AC converter uses the fixed frequency control to keep the system frequency equal to 60 Hz considering the optimal operation point of the diesel engine, and the output active power of DG is about 0.8 times rated power shown in Fig.9 (a). Therefore, the DG outputs constant active power and can operate the optimal point of fuel consumption efficiency. The active power balance between generation and load consumption is satisfied by the BUs when the load power changes. When the shipboard microgrid operates in Mode III, the shore power fixes the system frequency and the DC/AC converter uses droop control to facilitate connection into the shore power.

The *Q-V* droop control is used for the load reactive power sharing between the DC/AC converter and two DGs shown in Fig.9 (b) because we need to consider two aspects:

1) Load reactive power sharing and the voltage of different AC buses should be in the required range;

2) the capacity of the DC/AC converter and the power factor of the DG.

The droop control is implemented on the exciter of DGs like the automatic voltage regulator (AVR). The droop control of the DC/AC converter keeps the filter capacitor voltage in the required range.

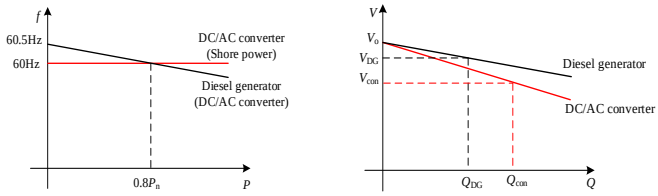

(a) *P-f.* (b) *V-Q*

Fig. 9. P-f &V-Q characteristics of DC/AC converter and DGs.

B. *Bidirectional DC/AC converter and its controller.*

The bidirectional DC/AC converter and its controller are shown in Fig.10. When the shipboard microgrid operates in Mode I, the three-loop controller is used to making the system frequency equal to 60 Hz and make the load voltage in the range. And in Mode II, the reactive power to voltage magnitude droop control plus virtual impedance is used to share the load reactive power between the DC/AC inverter and diesel engine. When the system operates in Mode III, active power to frequency droop is used to facilitate the DC/AC converter connection into the shore power.

In mode II, the coordinated control between the DC/AC converter and DGs makes the power factor of the diesel generators bigger than 0.9 and the reactive power sharing control is achieved by designing the droop gain and the value V_o with the virtual impedance. The inner loop is voltage and current control for maintaining the voltage of the filter capacitor in the required range and limitation the current of the filter inductor. The choice of controller parameters is based on the frequency bandwidth decoupling principle. The virtual impedance value is designed equally to the output impedance of the diesel generator.

This article has been accepted for publication in a future issue of this journal, but has not been fully edited. Content may change prior to final publication. Citation information: DOI 10.1109/TTE.2019.2928247, IEEE Transactions on Transportation Electrification

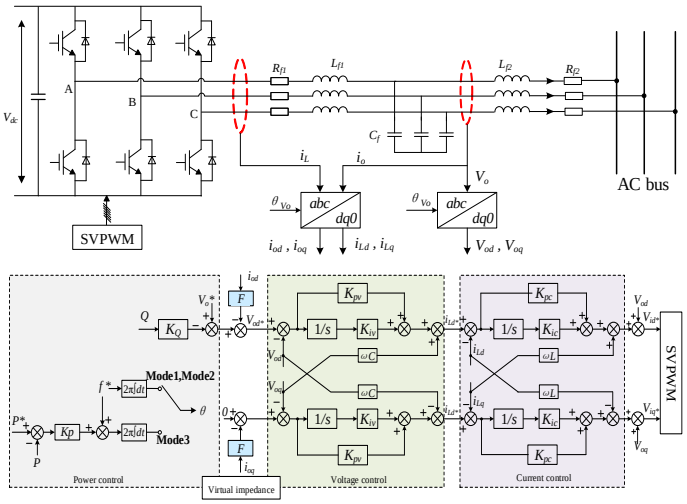

Fig.10. DC/AC converter and its controller.

In mode II, the diesel generators operate as a current source and the DC/AC converter operates as a voltage source. Therefore, the equivalent output impedance of the DC/AC converter can determine the maximum power of the diesel generator to the shipboard microgrid.

The dq axis DC/AC converter output voltage $\hat{v}_{od}$ and $\hat{v}_{oq}$ to the dq axis filter current can be expressed as:

$$\begin{aligned}\hat{v}_{od}(s)&=\hat{v}_{od}^{*}(s)\cdot G_{vc}-Z(s)\cdot\hat{i}_{od}(s)=(\hat{v}_{dd}(s)-\hat{i}_{od}(s)\cdot F)\cdot G_{vc}-Z(s)\cdot\hat{i}_{od}(s)\\&=\hat{v}_{dd}(s)\cdot G_{vc}-(F\cdot G_{vc}+Z(s))\cdot\hat{i}_{od}(s)\\\hat{v}_{oq}(s)&=\hat{v}_{oq}^{*}(s)\cdot G_{vc}-Z(s)\cdot\hat{i}_{oq}(s)=(\hat{v}_{dq}(s)-\hat{i}_{oq}(s)\cdot F)\cdot G_{vc}-Z(s)\cdot\hat{i}_{oq}(s)\\&=\hat{v}_{dq}(s)\cdot G_{vc}-(F\cdot G_{vc}+Z(s))\cdot\hat{i}_{oq}(s)\end{aligned}\tag{6}$$

Therefore, the equivalent output impedance can be expressed as:

$$Z_{VSC}=\begin{bmatrix}Z_{dd}(s) & Z_{dq}(s)\\ Z_{qd}(s) & Z_{qq}(s)\end{bmatrix}=\begin{bmatrix}Z(s)+F\cdot G_{vc} & \\ & Z(s)+F\cdot G_{vc}\end{bmatrix}\tag{7}$$

Where $G_{vc}(s)$, $Z(s)$ and $G_{ic}(s)$ can be expressed as equations (8) and (9).

$$\begin{aligned}G_{vc}(s)&=\frac{v_{odq}}{v_{odq}^{*}}=\frac{G_{vo}}{1+G_{vo}}=\frac{G_{ic}\cdot(K_{pv}+K_{iv}/s)}{C_f s+G_{ic}\cdot\dfrac{2}{(K_{pc}+K_{ic}/s)\cdot V_{dc}}+G_{ic}\cdot(K_{pv}+K_{iv}/s)}\\&=[(G_{ic}\cdot K_{pv}\cdot s+G_{ic}\cdot K_{iv})\cdot(K_{pc}\cdot V_{dc}\cdot s+K_{ic}\cdot V_{dc})]\\&\Big/[K_{pc}\cdot V_{dc}\cdot C_f\cdot s^3+(K_{ic}\cdot V_{dc}\cdot C_f+2G_{ic}+G_{ic}\cdot K_{pv}\cdot K_{pc}\cdot V_{dc})s^2\\&\quad+G_{ic}\cdot V_{dc}\cdot(K_{ic}\cdot K_{pv}+K_{pc}\cdot K_{iv})s+G_{ic}\cdot V_{dc}\cdot K_{ic}\cdot K_{iv}]\end{aligned}\tag{8}$$

$$\begin{aligned}Z(s)&=\frac{1}{C_f s+G_{ic}\cdot\dfrac{2}{(K_{pc}+K_{ic}/s)\cdot V_{dc}}+G_{ic}\cdot(K_{pv}+K_{iv}/s)}\\&=[V_{dc}\cdot(K_{pc}\cdot s+K_{ic})\cdot s]\\&\Big/[K_{pc}\cdot V_{dc}\cdot C_f\cdot s^3+(K_{ic}\cdot V_{dc}\cdot C_f+2G_{ic}+G_{ic}\cdot K_{pv}\cdot K_{pc}\cdot V_{dc})s^2\\&\quad+G_{ic}\cdot V_{dc}\cdot(K_{ic}\cdot K_{pv}+K_{pc}\cdot K_{iv})s+G_{ic}\cdot V_{dc}\cdot K_{ic}\cdot K_{iv}]\end{aligned}\tag{9}$$

$$G_{ic}(s)=\frac{i_{Ldq}}{i_{Ldq}^{*}}=\frac{(K_{pc}+K_{ic}/s)\cdot(V_{dc}/2)\cdot(1/L_{f1}s)}{1+(K_{pc}+K_{ic}/s)\cdot(V_{dc}/2)\cdot(1/L_{f1}s)}\tag{10}$$

The bode plots of the equivalent impedance $Z_0(s)=F\cdot G_{vc}(s)+Z(s)$ is shown in Fig.11. When the value of the virtual impedance increases, the damping $Z_0(s)$ increases. However, when the virtual impedance is large, the line voltage drop will also increase. We choose the value of the virtual impedance within the range of the allowed voltage drop.

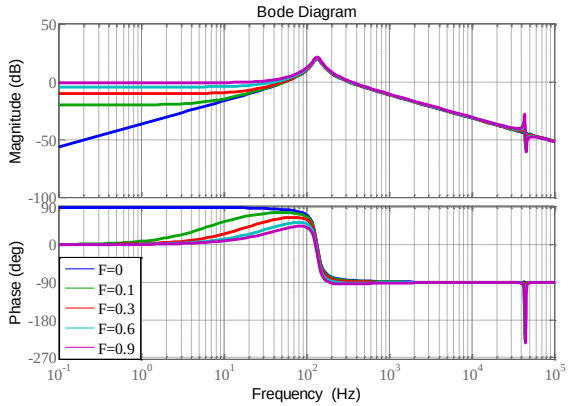

Fig.11. The bode plots of the equivalent impedance $Z_0(s)$.

C. *Diesel generator and its speed regulator and exciter.*

The 6-cylinder 2-stroke diesel engine is used and its mathematical model is in reference [37]. Two DGs and its speed regulator and exciter are shown in Fig.12. The control aim is to make the output active power of the DGs on the optimal point equal to $0.8P_{rated}$ and to share the load reactive power with the DC/AC converter by *Q-V* droop. *P-f* droop is for the synchronization control.

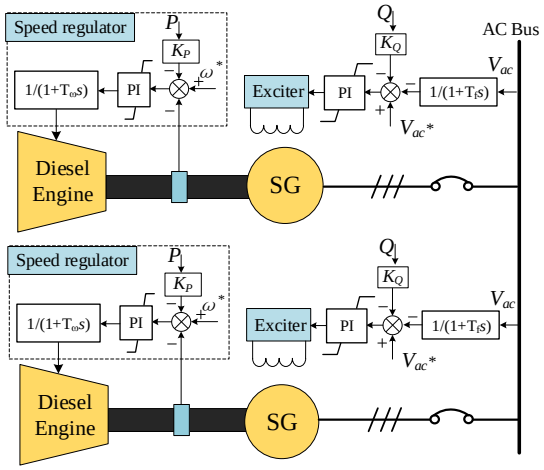

Fig.12. DGs and its speed regulator and exciter.

V. SHORE POWER MODE

When the hybrid electric ferry operates in shore power mode, the SPS is a grid-connected MG. The control aim is to synchronize and to charge the battery in the limited current. In this mode, the power control of the DC/AC converter is switched to Mode 3 and controlled by *P-f* droop shown in Fig.10. In this way, the shipboard microgrid is a controlled voltage source and supplies power to the hotel load before connecting to shore power; when connected to the shore power, it automatically becomes a controlled current source, charging the battery and supplying power to the hotel load. The DC/DC converter is to charge the battery units.

VI. SIMULATION RESULTS AND ANALYSIS

A. *Parameters of the hybrid electric ferry.*

A real hybrid-electric ferry is taken as a research case and the parameters are shown in TABLE II including the parameters of

This article has been accepted for publication in a future issue of this journal, but has not been fully edited. Content may change prior to final publication. Citation information: DOI 10.1109/TTE.2019.2928247, IEEE Transactions on Transportation Electrification

BUs, DC/DC converter and its controller, the DC bus, the bidirectional DC/AC converter, the diesel engine and its speed regulator, the diesel generator and its exciter, and the propulsion motor and its driver.

TABLE II PARAMETERS OF HYBRID ELECTRIC FERRY

BUs	**Value**
Rated voltage of battery /V	650
Battery capacity /Ah	160
Maximum charge current /A	160
Maximum discharge current /A	320
DC/DC converter and its controller	**Value**
Filter resistor/Ω	0.2
Filter inductor/mH	2
DC bus voltage	750
Switch frequency/Hz	8000
Outer voltage loop PI controller K_p, K_i	1,100
Inner current loop PI controller K_p, K_i	0.3,15
Anti-windup k_b	20
DC bus	**value**
DC bus voltage/V	750
Extra capacitor/mF	0
Capacitor for 4 converters/mF	4*1
Bidirectional DC/AC converter	**value**
Outer voltage loop PI controller K_p, K_i	0.1, 420.17
Inner current loop PI controller K_p, K_i	15,20000
RMS value of nominal phase to phase voltage/V	440
Rated frequency/Hz	60
Switch frequency/Hz	8000
Active power droop gain	0.8e-6
Reactive power droop gain	1.3e-5
Virtual impedance F	0.3
Reactive power reference	0
Diesel engine	**value**
Number of engine cycles	2
Number of cylinders	6
Rated capacity/kVA	88
Exciter	**value**
Q-V droop gain	1e-3
Rectifier smoothing time constant/s	0.002
Exciter time constant/s	0.002
Controller lag time constant/s	1
Diesel generator	**Value**
Nominal apparent power/ kVA	88
RMS value of nominal phase to phase voltage/V	440V
RMS value of nominal line current/A	200A
Nominal frequency/Hz	60 Hz
Nominal speed/rpm	900rpm
Pole pairs	4
d-axis synchronous reactance (X_d)/ p.u.	0.875
d-axis transient reactance (X_d')/ p.u.	0.19
d-axis subtransient reactance (X_d'')/ p.u.	0.136
q-axis synchronous reactance (X_q)/ p.u.	0.1625
q-axis subtransient reactance (X_q'') p.u.	0.135
Stator leakage reactance (X_l)/ p.u.	0.0163
d-axis transient time constant (T_{do}')/s	0.31
d-axis subtransient time constant (T_{do}'')/s	0.027
q-axis subtransient time constant (T_{qo}'')/s	0.01
Stator resistance (R_s)/ Ω	0.0056
Inertia constant (H)/s	0.5006117
Speed regulator	**value**
P-f droop gain	3.8e-5
PI controller	50,0
The inertia time constant of the actuator/s	8e-5
Maximum fuel intake	0.9095
Minimum fuel intake	0.00544
Propulsion motor and its driver	**value**
Rated power/kVA	150
Pole pairs	6
Stator resistance /Ω	0.00838
d-axis reactance /mH	0.37
q-axis reactance /mH	0.7
Voltage constant (V-peak L-L/rpm)	500
Inertia constant /kg.m^2	0. 63
Static Friction	0.001
Speed loop PI controller K_p, K_i	5, 5e-3
Inner current PI controller K_p, K_i	10, 1e-3

B. *Simulation results of different operation modes.*

Case1: Pure electric mode

TABLE III SIMULATION SCENARIOS OF MODE I

0-2s	Two propulsion motor is accelerated from 0 knots to 5 knots (800 rpm). And hotel loads power is 30kW.
2-7s	Two propulsion motors run at 5 knots.
7-9s	Two propulsion motor is accelerated from 5 knots to 8 knots.
9-15s	Two propulsion motors run at 8 knots (1300 rpm).
16-20s	Two propulsion motor is decelerated from 8 knots to 0 knots.

The simulation results of operation mode I are shown in Fig.13. The Fig.13 (a)-(c) show the rotation speed, mechanical torque and electromagnetic torque, active power of the propulsion motors. From the motor start, we know the mechanical torque of the propulsion motor is proportional to the square of the rotation speed.

Fig.13 (d) shows the DC bus voltage is in the required range when the load power changes.

The current and active power of BUs are shown in Fig.13 (g)-(i) that describes the discharging process of the BUs in pure electric mode.

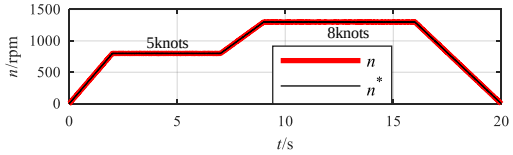

(a) Propulsion motor speed reference and motor speed.

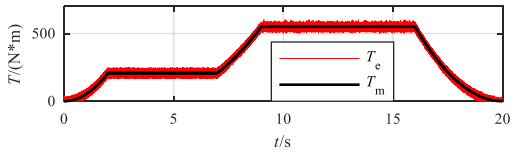

(b) Mechanical torque and electromagnetic torque of the propulsion motor.

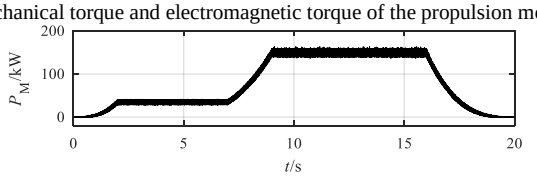

(c) Active power of PMSM1 and PMSG2.

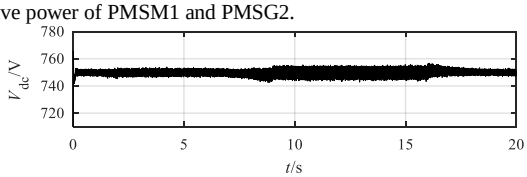

(d) DC bus voltage.

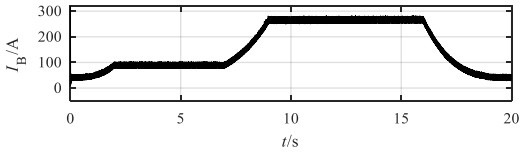

(g) BUs current.

This article has been accepted for publication in a future issue of this journal, but has not been fully edited. Content may change prior to final publication. Citation information: DOI 10.1109/TTE.2019.2928247, IEEE Transactions on Transportation Electrification

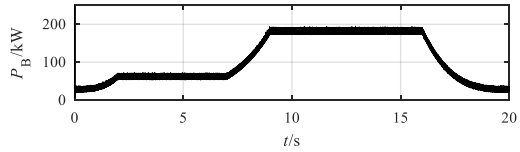

(i) BUs active power.

Fig. 13. Simulation results of the hybrid electric ferry in pure electric mode.

Case2: Range extended mode

TABLE IV SIMULATION SCENARIOS OF MODE II.

0-5s	Two propulsion motors run at 5 knots. One diesel generator is connected to SMG when the SoC of BUs is below 20%. The diesel generator outputs 70 kW active power. And hotel loads power is 30kW.
10-12s	Two propulsion motors are accelerated from 5 knots to 7 knots.
12s	Another diesel generator is connected at 12s and the output active power is 70kW.
12-20s	Two propulsion motors run at 7 knots (1100 rpm).

The simulation results of operation mode II are shown in Fig.14. The Fig.14 (a) shows the BUs SoC. The system frequency is shown in Fig.14 (b). When the 2th DG is connected to the AC bus, the system frequency has a little fluctuation and the maximum value is 60.2Hz. And then it is fixed to 60 Hz after the connection.

The Fig.14 (c)-(d) show the rotation speed and active power of the propulsion motors. The DC bus voltage is shown in Fig.14 (e) that when the DGs is connected to the system the DC bus voltage will have a required-range fluctuation and the start and power change of the propulsion motors have little effect on the DC bus voltage.

Fig.14 (f) shows the active power of the BUs, and the BUs is responsible for the power change balance between generation and consumption. From 12s, the BUs starts to charge. Fig.14 (g) and (h) show the output voltage magnitude of DC/AC converter and two DGs that is in the required range.

The output active & reactive power of the DC/AC converter is shown in Fig.14 (i) and (j). Before the first DG is connected to the SMG, the power flow of the DC/AC converter is from the BUs to the hotel loads. After that, the power flow is from the DGs to the propulsion motors.

Fig.14 (k) and (l) show the output active & reactive power of DGs. The active power of DGs is constant to make the diesel engine operate at the optimal point and the reactive power is almost zero to make the DG operate the unit power factor.

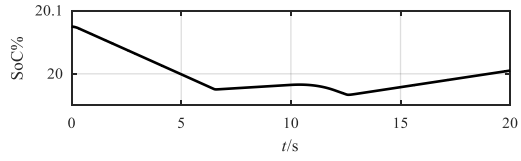

(a) BUs SoC.

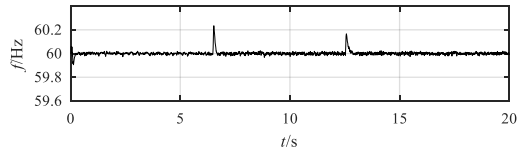

(b) System frequency.

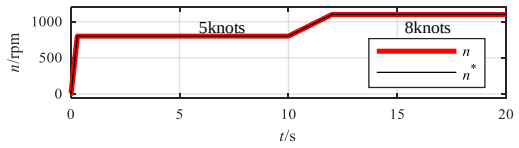

(c) Propulsion motor speed reference and motor speed.

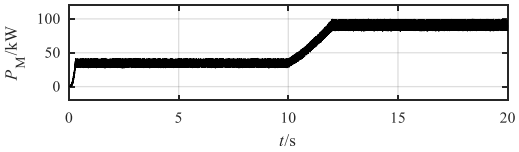

(d) The active power of PMSM1 and PMSG2.

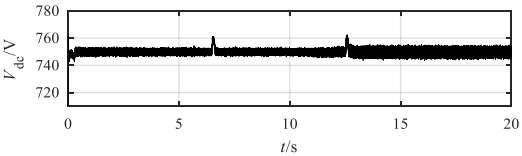

(e) DC bus voltage.

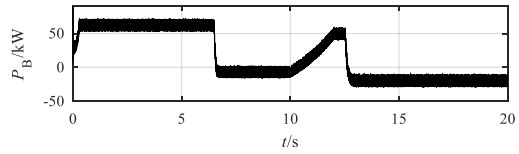

(f) BUs active power.

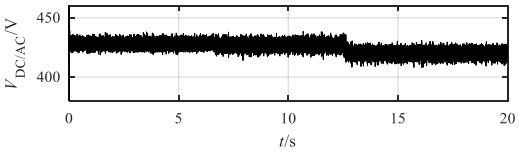

(g) Phase to phase voltage magnitude of DC/AC converter.

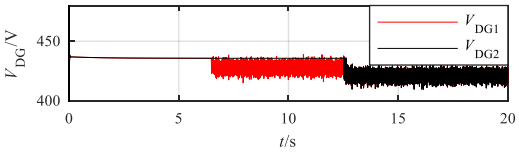

(h) Phase to phase voltage magnitude of DG1 and DG2.

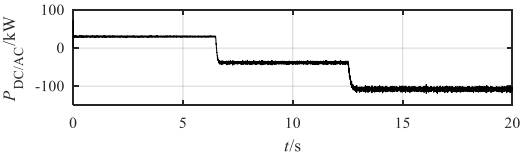

(i) Active power of DC/AC converter.

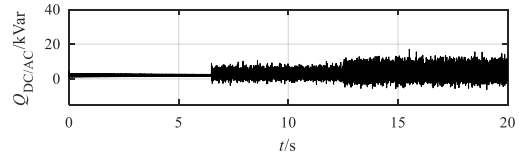

(j) Reactive power of DC/AC converter.

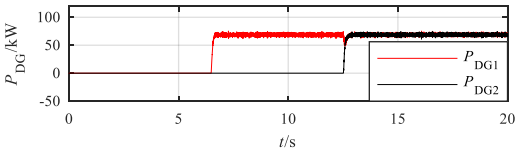

(k) Active power of DG1 and DG2.

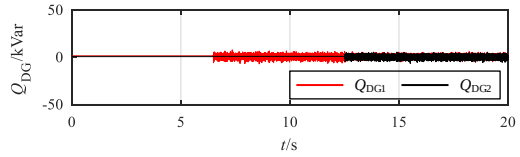

(l) Reactive power of DG1 and DG2

Fig. 14. Simulation results of the hybrid electric ferry in range extended mode.

Case3: Shore power mode

TABLE V SIMULATION SCENARIOS OF MODE III.

0-5s	The battery supplies hotel load, and propulsion motors and diesel generators stop. And hotel loads power is 30kW.
5s	The control mode of the DC/AC converter is switched from constant frequency control to droop control.
7-15s	The shipboard microgrid is connected to shore power at 7s.

The simulation results of operation mode III are shown in Fig.15. The Fig.15 (a) shows the BUs SoC. Before 7s, the BUs is discharged for the hotel load and after that, the BUs is charged by the shore power.

The system frequency is shown in Fig.15 (b). The control mode of the DC/AC converter is switched from constant frequency control to droop control at 5s that can facilitate the synchronous connection of the shipboard microgrid to the shore power.

The active power of BUs and the DC/AC converter are shown in Fig.15(c) that describes the charging process of the BUs in shore power mode.

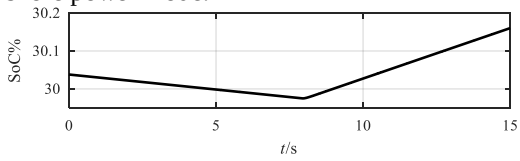

(a) BUs SoC.

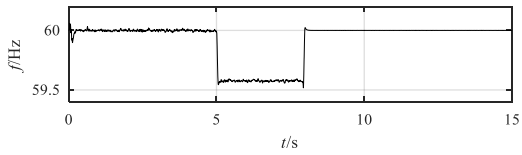

(b) System frequency.

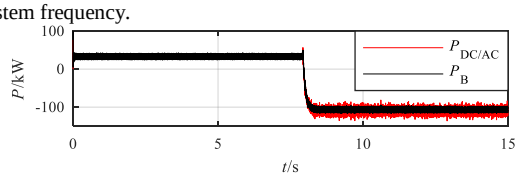

(e) Active power of DC/AC converter and BUs.

Fig. 15. Simulation results of the hybrid electric ferry in shore power mode.

VII. HARDWARE-IN-THE-LOOP RESULTS

In order to further verify the theoretical analysis results and the effectiveness of the proposed control strategy, a hardware-in-the-loop experiment based on dSPACE1006 is built. The experimental platform is shown in Fig.16.

Case1: Pure electric mode

The hardware-in-the-loop results of operation mode I are shown in Fig.17. The Fig.17 (a) shows the active power of the Bus, the propulsion motors and the hotel load. From the Fig.17 (a), we can see that the active power of the hotel load and propulsion motors is all provided by BUs in pure electric mode.

Fig.17 (b) shows that the DC bus voltage is in the required range and can quickly return to a steady state when the load power changes. The hardware-in-the-loop results are the same as the simulation results, they all prove the correctness of the control strategy.

Fig. 16. Experimental platform based on dSPACE1006 hardware-in-the-loop.

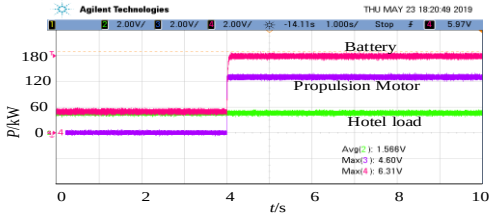

(a) Active power of Bus, PMSM and Hotel load.

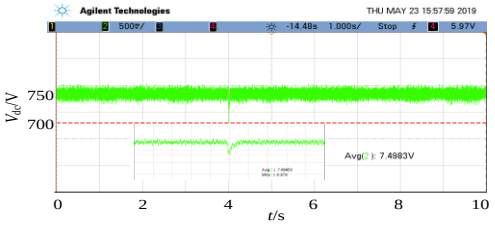

(b) DC bus voltage.

Fig. 17. Hardware-in-the-loop results of the hybrid electric ferry in pure electric mode.

Case2: Range extended mode

The hardware-in-the-loop results of operation mode II are shown in Fig.18. The Fig.18 (a) shows the active power of BUs, DG, PMSM and hotel load. In the beginning, the active power of the battery is supplied to the hotel load. In order to verify the effectiveness of the proposed control strategy, the propulsion motor is started at 4 s, and the battery still meets its active power requirements. At 7.4s, two synchronous generators are connected to provide 150kW constant power output. The battery changes from the discharge state to the charge state and the power reaches equilibrium again.

The Fig.18 (b) shows the output voltage magnitude of DC/AC converter and DG, same as simulation result they are also in the required range. The system frequency and the DC bus voltage are shown in Fig.18 (c) and (d), that means the system frequency and the DC bus voltage will have a required-range fluctuation when the DGs is connected to the system, furthermore, the start and power change of the propulsion motors have little effect on the system frequency and the DC

bus voltage. The hardware-in-the-loop results correspond to the simulation results, verifying the effectiveness of the control strategy.

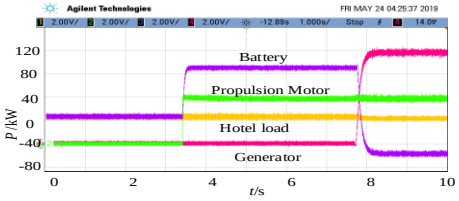

(a) Active power of BUs, DG, PMSM and Hotel load.

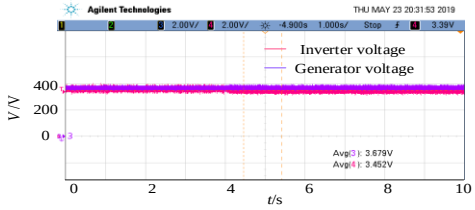

(b) Phase to phase voltage magnitude of DC/AC converter and DG

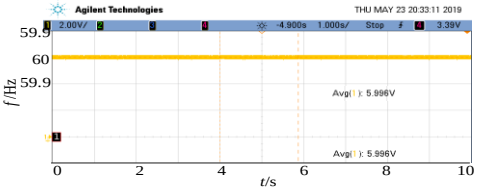

(c) System frequency.

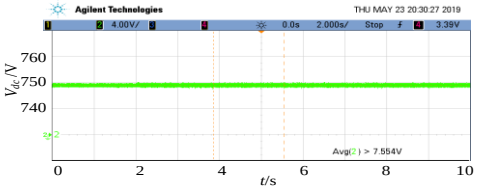

(d) DC bus voltage.

Fig. 18. Hardware-in-the-loop results of the hybrid electric ferry in range extended mode.

Case3: Shore power mode

The hardware-in-the-loop results of operation mode III are shown in Fig.19. Fig.19(a) shows the active power of BUs and the DC/AC converter. It is the same as the simulation result, which indicated there is low current stress in the process of connection between the system of the hybrid electric ferry and shore power by droop control. The system frequency is shown in Fig.19 (b). Compared to the simulation result, the hardware-in-the-loop result also illustrates that the control mode conversion of the DC/AC converter can facilitate the synchronous connection of the shipboard microgrid to the shore power.

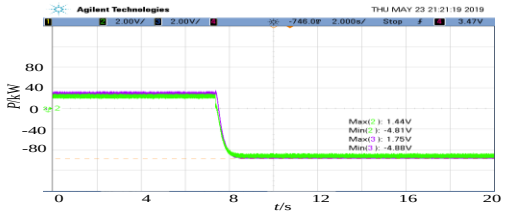

(a) Active power of DC/AC converter and BUs.

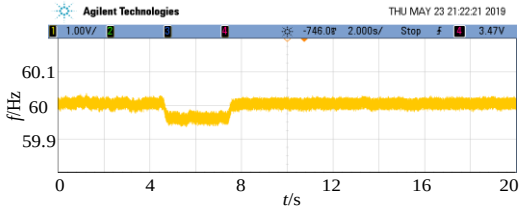

(b) System frequency.

Fig. 19. Hardware-in-the-loop results of the hybrid electric ferry in shore power mode.

VIII. CONCLUSION

In this paper, the power structure for a real hybrid-electric ferry and its coordinated control method are investigated. The power and control architecture presents the following features: 1) The designed power topology for the hybrid electric ferry in different operation modes. 2) The designed interleaved three-phase bidirectional DC/DC converter and its two-loop anti-windup PI controller can ensure the DC bus voltage and voltage ripple in the required range when the propulsion motors start and its power changes. The parameters of the DC bus capacitor and the controller are chosen by analyzing the stability of the boost DC/DC converter with its controller and the cascade system based on an impedance-based method. 3) The coordinated control between the DGs and the DC/AC converter can make the system frequency stable and get the optimal fuel efficiency of the diesel engines. And *Q-V* droop control plus a virtual impedance loop can achieve the load reactive power sharing, make each AC bus voltage in the required range and optimize the capacity of DC/AC converter and DGs. *P-f* droop facilitated the synchronization. 4) Achieve seamless transition among various operation scenarios.

REFERENCES

[1] Smith T W P, Jalkanen J P, Anderson B A, Corbett J J, Faber J, Hanayama S, Pandey A. Third IMO greenhouse gas study 2014[J]. Int. Marit. Organ, 2014, 327.

[2] Skjong E , Egil Rødskar, Molinas M , et al. The Marine Vessel's Electrical Power System: From its Birth to Present Day[J]. Proceedings of the IEEE, 2015, 103(12):2410-2424.

[3] Geertsma R D, Negenborn R R, Visser K, Hopman J J. Design and control of hybrid power and propulsion systems for smart ships: A review of developments[J]. Applied Energy, 2017, 194: 30-54.

[4] Chalfant J. Early-stage design for electric ship[J]. Proceedings of the IEEE, 2015, 103(12): 2252-2266.

[5] Wang F, Zhang Z, Ericsen T, Raju R, Burgos R, Boroyevich D. Advances in power conversion and drives for shipboard systems[J]. Proceedings of the IEEE, 2015, 103(12): 2285-2311.

[6] Dale S J, Hebner R E, Sulligoi G. Electric ship technologies[J]. Proceedings of the IEEE, 2015, 103(12): 2225-2228.

[7] Doerry N, Amy J, Krolick C. History and the status of electric ship propulsion, integrated power systems, and future trends in the US Navy[J]. Proceedings of the IEEE, 2015, 103(12): 2243-2251.

[8] Alexander D. Hybrid Electric Drive for Naval Combatants[J]. Proceedings of the IEEE, 2015, 103(12): 2267-2275.

[9] Kim S Y, Choe S, Ko S, Sul S K. A Naval Integrated Power System with a Battery Energy Storage System: Fuel efficiency, reliability, and quality of power[J]. IEEE electrification magazine, 2015, 3(2): 22-33.

[10] Yanamoto T, Izumi M, Yokoyama M, Umemoto K. Electric propulsion motor development for commercial ships in Japan[J]. Proceedings of the IEEE, 2015, 103(12): 2333-2343.

[11] Othman M, Anvari-Moghaddam A, Guerrero J M. Hybrid Shipboard Microgrids: System Architectures and Energy Management Aspects[C]//43rd Annual Conference of the IEEE Industrial Electronics Society (IECON'17). IEEE, 2017.

[12] McCoy T J. Integrated power systems—An outline of requirements and

functionalities for ships[J]. Proceedings of the IEEE, 2015, 103(12): 2276-2284.
[13] Prenc R, Cuculić A, Baumgartner I. Advantages of using a DC power system on board ship[J]. Pomorski zbornik, 2016, 52(1): 83-97.
[14] Zohrabi N, Shi J, Abdelwahed S. An overview of design specifications and requirements for the MVDC shipboard power system[J]. International Journal of Electrical Power & Energy Systems, 2018, 104: 680-693.
[15] Davey K, Hebner R E. Power Grid for a Naval Electric Ship-AC versus DC[J]. CEM Publications, 2015.
[16] Hansen J F, Lindtjørn J O, Myklebust T, et al. Onboard DC grid[J]. ABB, 2012.
[17] Jin Z, Sulligoi G, Cuzner R, Meng L, Vasquez J C, Guerrero J M. Next-generation shipboard dc power system: Introduction smart grid and dc microgrid technologies into maritime electrical networks [J]. IEEE Electrification Magazine, 2016, 4(2): 45-57.
[18] Zahedi B, Norum L E, Ludvigsen K B. Optimized efficiency of all-electric ships by dc hybrid power systems[J]. Journal of power sources, 2014, 255: 341-354.
[19] Zahedi B. Shipboard DC Hybrid Power Systems: Modeling, efficiency analysis and stability control[D]. 2014.
[20] Bassam A, Phillips A, Turnock S, Wilson P A. Design, modeling and simulation of a hybrid fuel cell propulsion system for a domestic ferry[J]. 2016.
[21] Guerrero J M, Vasquez J C, Matas J, De Vicuña L G, Castilla M. Hierarchical control of droop-controlled AC and DC microgrids—A general approach toward standardization[J]. IEEE Transactions on industrial electronics, 2011, 58(1): 158-172.
[22] Hebner R E, Uriarte F M, Kwasinski A, et al. Technical cross-fertilization between terrestrial microgrids and ship power systems[J]. Journal of Modern Power Systems and Clean Energy, 2016, 4(2): 161-179.
[23] Ginn H L, Hingorani N, Sullivan J R, Wachal R. Control Architecture for High Power Electronics Converters[J]. Proceedings of the IEEE, 2015, 103(12): 2312-2319.
[24] Hebner R E, Davey K, Herbst J, Hall D, Hahne J, Surls D D, Ouroua A. Dynamic load and storage integration[J]. Proceedings of the IEEE, 2015, 103(12): 2344-2354.
[25] Al-Falahi M D A, Nimma K S, Jayasinghe S D G, Enshaei H, Guerrero J M. Power management optimization of hybrid power systems in electric ferries[J]. Energy Conversion and Management, 2018, 172: 50-66.
[26] Wang X, Wang C, Xu T, et al. Optimal voltage regulation for distribution networks with multi-microgrids[J]. Applied Energy, 2018, 210: 1027-1036.
[27] Zhong Q C. Robust droop controller for accurate proportional load sharing among inverters operated in parallel[J]. IEEE Transactions on Industrial Electronics, 2013, 60(4): 1281-1290.
[28] He L, Li Y, Shuai Z, Guerrero J M, Cao Y, Wen M, Shi J. A Flexible Power Control Strategy for Hybrid AC/DC Zones of Shipboard Power System with Distributed Energy Storages[J]. IEEE Transactions on Industrial Informatics, 2018.
[29] Liu Y, Guo L, Wang C. A robust operation-based scheduling optimization for smart distribution networks with multi-microgrids[J]. Applied Energy, 2018, 228: 130-140.
[30] Al-Falahi M, Tarasiuk T, Jayasinghe S, Jin Z, Enshaei H, Guerrero J. AC ship microgrids: control and power management optimization[J]. Energies, 2018, 11(6): 1458.
[31] Jin Z, Meng L, Guerrero J M, Han R. Hierarchical Control Design for a Shipboard Power System With DC Distribution and Energy Storage Aboard Future More-Electric Ships[J]. IEEE Transactions on Industrial Informatics, 2018, 14(2): 703-714.
[32] Kanta S, Plangklang B, Subsingha W. Design of a Bi-directional DC-DC 4 phase Interleave converter for PV applications[J]. Energy Procedia, 2014, 56: 604-609.
[33] Jin Z, Meng L, Guerrero J M. Constant Power Load Instability Mitigation in DC Shipboard Power Systems Using Negative Series Virtual Inductor Method[C]//43rd Annual Conference of IEEE Industrial Electronics Society (IECON 2017). 2017.
[34] Ahmadi R, Paschedag D, Ferdowsi M. Closed-loop input and output impedances of DC-DC switching converters operating in voltage and current mode control[C]//IECON 2010-36th Annual Conference on IEEE Industrial Electronics Society. IEEE, 2010: 2311-2316.
[35] Na Z, Hui Z, Xi X. System-level stability analysis of DC microgrid with distributed control strategy[C]//Proceedings of the CSEE. 2016, 36(2): 368-378.
[36] Rahimi A M, Emadi A. Active damping in DC/DC power electronic converters: A novel method to overcome the problems of constant power loads[J]. IEEE Transactions on Industrial Electronics, 2009, 56(5): 1428-1439.
[37] Anderson P M, Mirheydar M. Analysis of a diesel-engine driven generating unit and the possibility for voltage flicker[J]. IEEE transactions on energy conversion, 1995, 10(1): 37-47.

Xiao Zhaoxia received the B.S. degree in Electrical Engineering and Automation, Hebei University of Technology, the M.S. degree in Control Theory and Control Engineering, and the Ph.D. degree in Power System and its Automation from Tianjin University, Tianjin, P. R. China, in 2002, 2005 and 2008, respectively. From 2007-2008, she studied in University of Manchester, UK as a Ph.D. Guest. Since 2009, she began to work in Tianjin Polytechnic University. She has been an associate professor and Professor from 2011,2018. From Sep. 2012 to Dec. 2012 she was a Visiting Scholar in Fraunhofer IWES, Germany. From Dec.2016 to Jan.2018, she was a Visiting Scholar in Department of Energy Technology, Aalborg University, Denmark. Her research interests include AC/DC Microgrids with renewable energy, maritime microgrids, planning of distribution network. She has authored and co-authored more than 30 technical papers in Microgrids conferences and journals.

Zhu Tian-li received the B.S. degree in Electrical Engineering and Automation, Tianjin Polytechnic University, Tianjin, China, in 2015. Currently, he working toward the M.E. degree. His research interests include AC/DC Microgrids with renewable energy, and maritime microgrids.

Li Huai-min received the B.S. degree in Electrical Engineering and Automation, Tianjin Polytechnic University, Tianjin, China, in 2017. He is currently working toward the M.E. degree. His research interests include control of power electronic converters, DC Microgrids, and their applications in maritime microgrids.

Josep M. Guerrero (S'01-M'04-SM'08-FM'15) received the B.S. degree in telecommunications engineering, the M.S. degree in electronics engineering, and the Ph.D. degree in power electronics from the Technical University of Catalonia, Barcelona, in 1997, 2000 and 2003, respectively. Since 2011, he has been a Full Professor with the Department of Energy Technology, Aalborg University, Denmark, where he is responsible for the Microgrid Research Program (www.microgrids.et.aau.dk). From 2014 he is chair Professor in Shandong University; from 2015 he is a distinguished guest Professor in Hunan University; and from 2016 he is a visiting professor fellow at Aston University, UK, and a guest Professor at the Nanjing University of Posts and Telecommunications. From 2019, he became a Villum Investigator by The Villum Foundation, which supports the Centre for Research on Microgrids (CROM) at Aalborg University, being Prof. Guerrero the founder and Director of the same centre.

His research interests is oriented to different microgrid aspects, including power electronics, distributed energy-storage systems, hierarchical and cooperative control, energy management systems, smart metering and the internet of things for AC/DC microgrid clusters and islanded minigrids. Specially focused on maritime microgrids for electrical ships, vessels, ferries and seaports. Prof. Guerrero is an Associate Editor for a number of IEEE TRANSACTIONS. He has published more than 500 journal papers in the fields of microgrids and renewable energy systems, which are cited more than 30,000 times. He received the best paper award of the IEEE Transactions on Energy Conversion for the period 2014-2015, and the best paper prize of IEEE-PES in 2015. As well, he received the best paper award of the Journal of Power Electronics in 2016. During five consecutive years, from 2014 to 2018, he was awarded by Clarivate Analytics (former Thomson Reuters) as Highly Cited Researcher. In 2015 he was elevated as IEEE Fellow for his contributions on "distributed power systems and microgrids."

Chun-Lien Su (M'01-SM'13) received the Diploma degree in Electrical Engineering from National Kaohsiung Institute of Technology, Taiwan, the M.S. and Ph.D. degrees in Electrical Engineering from the National Sun Yat-Sen University, Taiwan in 1992, 1997, and 2001, respectively. In 2002 and 2006, he was Assistant Professor and Associate Professor at the Department of Marine Engineering, National Kaohsiung Marine University, Taiwan, respectively. Since 2012, he has been as a Full Professor where he is the Director at the Energy and Control Research Center. From Aug. 2017 to Jan. 2018 he was a Visiting Professor at the Department of Energy Technology, Aalborg University, Denmark and is now Professor in National Kaohsiung University of Science and Technology. His research interests include power system analysis and computing, power quality, maritime microgrids, and offshore energy; recently specially focused on electrical infrastructure for offshore wind farms and maritime microgrids for electrical ships, vessels, ferries and seaports. He has been Guest Editor of the IEEE TRANSACTIONS ON INDUSTRIAL INFORMATICS Special Issues: Next Generation Intelligent Maritime Grids. He received the best paper prize of the Industrial & Commercial Power Systems Conference at IEEE-IAS for the period 2012-2013, and the best paper award of IEEE International Conference on Smart Grid and Clean Energy Technologies in 2018.

Juan C. Vasquez (M'12-SM'14) received the B.S. degree in electronics engineering from the Autonomous University of Manizales, Manizales, Colombia, and the Ph.D. degree in automatic control, robotics, and computer vision from BarcelonaTech-UPC, Spain, in 2004 and 2009, respectively. He was with the Autonomous University of Manizales working as a teaching assistant and the Technical University of Catalonia as a Post-Doctoral Assistant in 2005 and 2008. In 2011, He was Assistant Professor and in 2014 He was an Associate Professor at the Department of Energy Technology, Aalborg University, Denmark. In 2019, He became a Full Professor and currently He is the Vice Programme Leader of the Microgrids Research Program (see microgrids.et.aau.dk). He was a Visiting Scholar at the Center of Power Electronics Systems (CPES) at Virginia Tech and a visiting professor at Ritsumeikan University, Japan. His current research interests include operation, advanced hierarchical and cooperative control, optimization and energy management applied to distributed generation in AC/DC Microgrids, maritime microgrids, advanced metering infrastructures and the integration of Internet of Things and Energy Internet into the SmartGrid. Dr Vasquez is a Associate Editor of IET POWER ELECTRONICS and a Guest Editor of the IEEE TRANSACTIONS ON INDUSTRIAL INFORMATICS Special Issue on Energy Internet. In 2017 and 2018, Dr. Vasquez was awarded as Highly Cited Researcher by Thomson Reuters and in 2019, He was the recipient of the Young Investigator Award 2019. He has published more than 300 journal papers in the field of Microgrids, which in total are cited more than 15000 times. Dr. Vasquez is currently a member of the IEC System Evaluation Group SEG4 on LVDC Distribution and Safety for use in Developed and Developing Economies, the Renewable Energy Systems Technical Committee TC-RES in IEEE Industrial Electronics, PELS, IAS, and PES Societies.